BNL-211351-2019-JAAM

Chemical synthesis of magnetically hard and strong rare-earth metal based nanomagnets

B. Shen, D. Su

To be published in "Angewandte Chemie"

November 2018

Center for Functional Nanomaterials

Brookhaven National Laboratory

U.S. Department of Energy

USDOE Office of Science (SC), Basic Energy Sciences (BES) (SC-22)

DISCLAIMER

Chemical synthesis of magnetically hard and strong rare-earth metal based nanomagnets

Bo Shen, Chao Yu, Alexander A. Baker, Scott K. McCall, Yongsheng Yu, Dong Su, Zhouyang Yin, Hu Liu, Junrui Li and Shouheng Sun*

Abstract: We report a general chemical approach to synthesize strongly ferromagnetic rare earth metal (REM) based SmCo and SmFeN nanoparticles (NPs) with ultra-large coercivity. The synthesis started with the preparation of hexagonal CoO + Sm_2O_3 (denoted as SmCo-O) multipods via decomposition of $Sm(acac)_3$ and $Co(acac)_3$ in oleylamine. These multipods were further reduced with Ca at 850 °C to form $SmCo_5$ NPs with sizes tunable from 50 to 200 nm. The 200 nm $SmCo_5$ NPs were dispersed in ethanol, and magnetically aligned in polyethylene glycol (PEG) matrix, yielding a PEG-$SmCo_5$ NP composite with the room temperature coercivity (H_c) of 49.2 kOe, the largest H_c among all ferromagnetic NPs ever reported, and saturated magnetic moment (M_s) of 88.7 emu/g, the highest value reported for $SmCo_5$ NPs. The method was extended to synthesize other ferromagnetic NPs of Sm_2Co_{17}, and, for the first time, of $Sm_2Fe_{17}N_3$ NPs with H_c over 15 kOe and M_s reaching 127.9 emu/g. These REM based NPs are important magnetic building blocks for fabrication of high performance permanent magnets, flexible magnets, and printable magnetic inks for energy and sensing applications.

The synthesis of magnetically “hard” and “strong” nanoparticles (NPs) is an essential first step towards development of ultra-strong magnets for broad renewable energy, magnetic, electronic, and medical applications.[1] Past studies have shown the possibility of preparing monodisperse magnetic NPs with coercivity surpassing 10 kOe (1 Oe = 79.58 A/m), but these NPs are often FePt-based and thus have limited uses outside special applications due to material costs.[2] Rare-earth metal (REM) based NdFeB, SmCo, and SmFeN magnets have magnetic characteristics that are similar or superior to the FePt systems and are the materials of choice for hard magnetic NPs.[3] However, to prepare REM NPs with controlled sizes and magnetic properties has been extremely challenging due to the chemical instability of the REM.[4] Here we report a high yield (up to 85%) chemical synthesis of magnetically hard and strong SmCo and SmFeN NPs with sizes tunable from 50 to 200 nm. These NPs are dispersible in ethanol, enabling their alignment in polyethylene glycol (PEG) matrix. The aligned 200 nm $SmCo_5$ NPs have a room temperature coercivity (H_c) of 49.2 kOe, the largest value among all ferromagnetic NPs ever reported,[5] and saturated magnetic moment (M_s) of 88.7 emu/g, the highest value reported on $SmCo_5$ NPs.[6] Our method overcomes the known problems of low yield, wide NP size distribution, and NP sintering observed from previous syntheses and provides a general way of producing REM based nanomagnets for magnetic and electronic applications.

The key to the successful preparation of hexagonal SmCo NPs is a new method to prepare hexagonal CoO + Sm_2O_3 (denoted as SmCo-O) within one nanostructure through 230°C reductive decomposition of $Co(acac)_3$ and $Sm(acac)_3$ (acac = acetylacetonate) with oleylamine as both solvent and surfactant (Supporting Information, SI). This reaction condition was chosen to avoid further reduction of CoO to metallic Co,[7] and to initiate the formation of Sm_2O_3.[6a] Sm/Co ratios were controlled by the amount of $Sm(acac)_3$ and $Co(acac)_3$ added in the reaction mixture. For example, to prepare SmCo-O that can be used to synthesize $SmCo_5$, the Sm/Co molar ratio in SmCo-O was controlled to be 1:4.5. After three hours of reaction, SmCo-O multipods, as shown in transmission electron microscopy (TEM) images (Figure 1), were obtained in 90% yield with the pod dimensions controlled by $Co(acac)_3$ concentration – 25 mM, 50 mM, and 100 mM $Co(acac)_3$ yielded respectively 60 (±10) x 10 (±3) nm (Figure 1a); 110 (±20) x 25 (±5) nm (Figure 1b), and 220 (±40) x 45 (±5) nm multipods (Figure 1c). X-ray diffraction (XRD) shows that the SmCo-O multipods have a hexagonal wurtzite structure of CoO without showing obvious Sm_2O_3 diffraction peaks (Figure 1d & Figure S1). High resolution TEM (HRTEM) (Figure 1e) shows that the (002) lattices (fringe distance of 0.260 nm) stacks along the long axis of the rod, suggesting that CoO nanorods are formed by growing CoO along the [001] direction. To confirm that Sm-O is present in the multipod structure, we analyzed the 110 nm SmCo-O pods by high-angle annular dark-field scanning TEM (HAADF-STEM) and elemental mapping (Figure 1f). From the images, we can see that Sm (red), Co (blue) and O (green) elements distributed across the multipod structure. Inductively coupled plasma-atomic emission spectroscopy (ICP-AES) analysis further confirms that in the SmCo-O NPs, the ratio of Sm/Co is at 1:4.5. These studies indicate that Sm_2O_3 is indeed present in the SmCo-O NP structure, but it is in an amorphous state, forming a mixture with the crystalline CoO. The multipod morphology is formed likely from the kinetic growth of hexagonal CoO nanorods.[8] This fast kinetic growth process also causes the nanorods to share a joint, forming a multipod structure.[9] Small Sm-O particles are embedded in the pod structure. Such a hexagonal CoO dominated multipod structure provides a unique precursor for the formation of hexagonal $SmCo_5$.

[a] Dr. B. Shen, Dr. C. Yu, Z. Yin, H. Liu, J. Li and Prof. S. Sun
Department of Chemistry, Brown University
Providence, RI, 02912 (USA)
E-mail: ssun@brown.edu
[b] Dr. A. A. Baker, Dr. S. K. McCall
Materials Science Division, Lawrence Livermore National Laboratory.
Livermore, CA, 94550 (USA)
[b] Prof. Y. Yu, H. Liu
School of Chemical Engineering and Technology, Harbin Institute of Technology
Harbin, Heilongjiang, 150001 (China)
[b] Dr. D. Su
Center for Functional Nanomaterials, Brookhaven National Laboratory
Upton, NY, 11973 (USA)

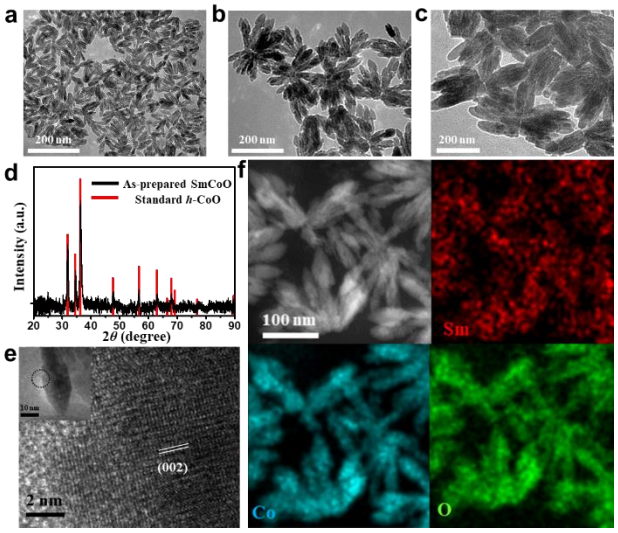

Figure 1. TEM images of as-synthesized a) 60 nm b) 110 nm c) 220 nm SmCo-O multipods. d) XRD patterns of SmCo-O multipods and standard hexagonal CoO pattern (JPCDS No. 80-0075). e) HRTEM image of an enlarged part of a SmCo-O nanorod (inserted). The crystal lattice matches well to (002) facets of hexagonal CoO structure. f) HADDF-STEM image and elemental mapping of Sm (red), Co (blue) and O (green) of 110 nm SmCo-O multipods.

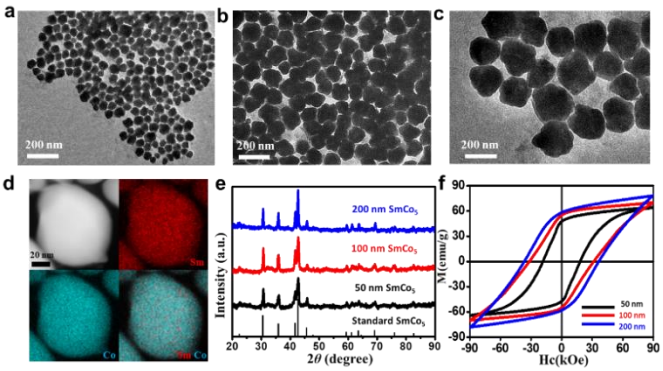

Figure 2. TEM images of a) 50 nm b) 100 nm c) 200 nm $SmCo_5$ NPs. d) HADDF-STEM image of a 100 nm $SmCo_5$ NP and elemental mapping showing Sm (red) and Co (blue) distribution across the NP. e) XRD patterns of $SmCo_5$ NPs and standard $SmCo_5$ pattern (JPCDS No. 65-8981). f) Hysteresis loops of as-synthesized and unaligned 50 nm, 100 nm and 200 nm $SmCo_5$ NPs at 300 K.

To prepare $SmCo_5$, we first embedded the $SmCo_{4.5}$-O multipods into a CaO matrix by precipitating $Ca(acac)_2$ with hexadecyltrimethylammonium hydroxide in the presence of SmCo-O dispersed in 1-octadecene at 200 °C (SI) (Figure S2). We further annealed the SmCo-O/CaO composite in air at 185 °C for 5 h to ensure the tighter coating of CaO around SmCo-O (to prevent $SmCo_5$ phase from sintering) and to remove organics in the composite (to avoid any undesirable formation of CoC_x[10]) in the next step reduction process.[11] To reduce SmCo-O to $SmCo_5$, the SmCo-O/CaO was ground together with metallic Ca and then annealed at 850 °C for 30 min to convert 60 nm, 110 nm, and 220 nm SmCo-O multipods to 50 nm, 100 nm, and 200 nm $SmCo_5$ NPs respectively. CaO and Ca residue in the powder product was removed by washing the annealed powder with NH_4Cl methanol solution. This washing step, compared with conventional water washing,[12] can also help to reduce the thickness of oxide layers on the metal NP surface.[5c] Figure 2a-c show the TEM images of 50 ± 10 nm, 100 ± 20 nm and 200 ± 30 nm $SmCo_5$ NPs, respectively. HAADF-STEM image and elemental mapping of a typical 100 nm particle show Sm and Co distribute evenly in the particle (Figure 2d). The XRD patterns of these three kinds of $SmCo_5$ NPs match well with the standard hexagonal D_{2d} intermetallic $SmCo_5$ phase (Figure 2e). The Sm/Co ratio was measured by ICP-AES to be 1/5. Magnetic properties of the $SmCo_5$ NPs were characterized by a vibrating sample magnetometer at room temperature. The hysteresis loops show these $SmCo_5$ NPs are all strongly ferromagnetic at 300 K, but they cannot be saturated under the current 90 kOe field strength, showing only minor loops with larger NPs being magnetically harder and stronger (Figure 2f).

One important feature of our synthesis is that the $SmCo_5$ NPs obtained from the annealing step can be dispersed in a solvent and be embedded in a polymer under an external magnetic field, forming a $SmCo_5$-polymer composite with $SmCo_5$ NPs becoming magnetically aligned. For example, under a N_2 atmosphere, we dispersed $SmCo_5$ NPs in ethanol and mixed them with polyethylene glycol (PEG) (NPs/PEG mass ratio is 1:5). After ethanol evaporation in a 10 kOe field, the composite was placed in a stronger 90 kOe field and was heated to 370 K to melt PEG and to allow NPs to further align with the magnetic field direction. The sample was cooled to room temperature, freezing NP alignment in the PEG matrix. Figure 3a&b show HRTEM images of two representative $SmCo_5$ NP aligned in the out-of-plane (Figure 3a) and in-plane direction (Figure 3b). The lattice fringes shown in Figure 3a have an average spacing of 0.216 nm, corresponding to the interplanar spacing of (200) planes. The hexagonal fringe pattern is obtained from the $SmCo_5$ crystal lattice projected along [001] zone axis. Figure 3b shows two different lattice fringes with the spacing of 0.249 and 0.198 nm, matching with the interplanar spacing of (110) and (002) respectively with (002) aligning in the image plane and perpendicular to the (110). The oxidation layer over the PEG protected $SmCo_5$ NPs is about 2 nm, which is thinner than the 5 nm layer observed in the as-synthesized $SmCo_5$ NPs separated from ethanol dispersion (Figure S3), indicating that PEG matrix can provide more efficient stabilization of $SmCo_5$ NPs against surface oxidation by air. Also, TEM image shows the NPs in the aligned PEG-$SmCo_5$ tend to pack along the magentic field direction (Figure S4), implying that there exists a strong NP interaction, which helps to improve the NP magentic performance. The aligned 200 nm $SmCo_5$ NPs have an almost square hysteresis behavior (Figure 3c) with H_c of 49.2 kOe, M_s at 88.7 emu/g and M_r at 82.9 emu/g (M_r/M_s ratio = 0.93). This magnetization value is only 14% less than that from the bulk $SmCo_5$ (99 emu/g).[13] This H_c is largest value ever reported for magnetic NPs and M_s is the highest values for $SmCo_5$ NPs. Furthermore, we studied temperature (210 - 330 K) dependent demagnetization behavior of the aligned 200 nm $SmCo_5$ NPs (Figure 3d). Their H_c decreases from 64.5 kOe at 210 K to 40.9

kOe at 330 K due to the temperature dependence of magnetocrystalline anisotropy energy of the hexagonal $SmCo_5$ structure.[14] However, their M_s shows little change in this temperature range, which is especially important for magnetic applications at different temperatures. Similarly, the 50 nm and 100 nm SmCo NPs can also be aligned with their H_c at 25.3 kOe and 44.5 kOe, and M_s at 80.9 emu/g and 84.2 emu/g, respectively, which shows a size-dependent magnetic property (Figure 3c).

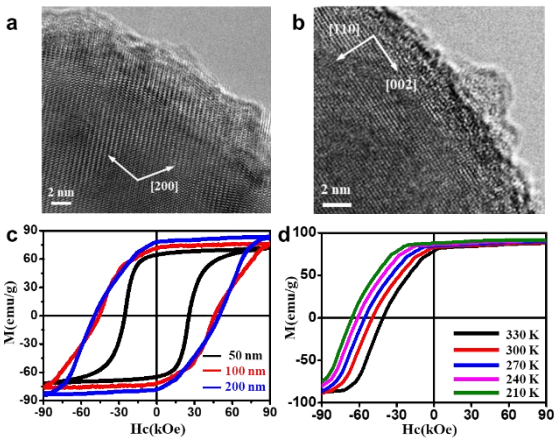

Figure 3. HRTEM of representative $SmCo_5$ NPs aligned from a) out-of-plane and b) in-plane direction. c) Hysteresis loops of 50 nm, 100 nm and 200 nm $SmCo_5$ NPs after external field alignment and embedded in PEG at 300 K. d) Demagnetization curves at select temperatures for the aligned 200 nm PEG-$SmCo_5$ composite.

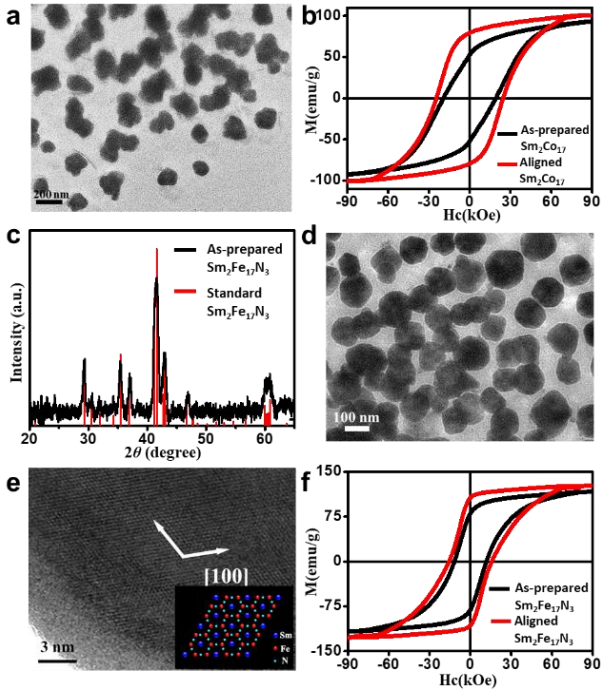

Figure 4. a) TEM image of 100 nm Sm_2Co_{17} NPs. b) Hysteresis loops of as-synthesized and aligned Sm_2Co_{17} NPs at 300 K. c) XRD of as-prepared $Sm_2Fe_{17}N_3$ NPs (black curve) and the standard pattern of rhombohedral structure $Sm_2Fe_{17}N_3$ (red lines, JPCDS No. 00-048-1790). d) TEM image of 100 nm $Sm_2Fe_{17}N_3$ NPs. e) HRTEM image of a $Sm_2Fe_{17}N_3$ NP (insert: atomic model of the $Sm_2Fe_{17}N_3$ structure projected along the *c*-axis.). f) Hysteresis loops of as-synthesized and aligned $Sm_2Fe_{17}N_3$ NPs at 300 K.

By adjusting the initial ratio of $Sm(acac)_3/Co(acac)_3$ to be 1/8 in the reaction, we obtained 120 (±20) nm hexagonal CoO + Sm_2O_3 (denoted as $SmCo_8$-O) NPs (Fig S5). Note that, in this process, hexagonal CoO tends to grow into pyramidal shape due to the presence of smaller amount of $Sm(acac)_3$, consistent with reports on the additive-induced shape control of CoO.[8] Using the same CaO coating, annealing, and magnetic alignment processes as described in the synthesis of $SmCo_5$ NPs, we obtained 100 (±20) nm Sm_2Co_{17} NPs with hexagonal intermetallic phase (Figure 4a&S6), which are strongly ferromagnetic with their H_c reaching 24.2 kOe and M_s at 100.5 emu/g (Figure 4b) (M_s of bulk Sm_2Co_{17} is 112 emu/g.[13]). Both H_c and M_s are among the highest values ever reported for Sm_2Co_{17} obtained from any other methods.[15]

Our synthetic method can be extended further to prepare hard magnetic $Sm_2Fe_{17}N_3$ NPs. Compared with NdFeB and SmCo magnets, SmFeN has a higher energy product (472 kJ/m^3) than $SmCo_5$ (219 kJ/m^3), and higher Curie temperature (749 K) than NdFeB (588 K), making it promising as a high performance magnet at temperatures up to 520 K. However, nanostructured $Sm_2Fe_{17}N_3$ is rarely studied due to the difficulty of stabilizing the meta-stable $Sm_2Fe_{17}N_3$ phase, which is conventionally obtained by high pressure nitridation of Sm_2Fe_{17} in the presence of N_2 or NH_3.[16] Here, we modified the synthesis of Sm_2Co_{17} NPs by replacing $Co(acac)_3$ with $Fe(acac)_3$, adding oleic acid at 230 °C, then raising the reaction temperature to 300 °C (SI), and obtained 110 (±20) nm cubic structure SmFe-O (Figure S7). Using the same CaO coating and reductive annealing process as described in the preparation of $SmCo_5$ NPs, we obtained rhombohedral Sm_2Fe_{17} NPs that are weakly ferromagnetic (Figure S8). These Sm_2Fe_{17} NPs were nitridated at ambient pressure in the presence of melamine ($C_3H_6N_6$) at 600 °C (SI) to form 100 (±20) nm rhombohedral structure $Sm_2Fe_{17}N_3$ NPs (Figure 4c&d). Note that 600 °C is the maximum temperature that can be used to prepare stable $Sm_2Fe_{17}N_3$ NPs. Annealed at 650 °C, these NPs decompose to SmN + Fe (Figure S9). In this process, no metal carbides could be detected. HRTEM image of a part of a $Sm_2Fe_{17}N_3$ NP shows the lattice fringe spacing of 0.262 nm in the core (oxide shell about 4 nm) that corresponds to the (300) lattice spacing of $Sm_2Fe_{17}N_3$ (Figure 4e). The lattice pattern matches with the atom model built along *c*-axis of $Sm_2Fe_{17}N_3$ crystal lattice.

The $Sm_2Fe_{17}N_3$ NPs are strongly ferromagnetic and have a room temperature H_c of 15.4 kOe and M_s of 127.9 emu/g (Figure 4f). The synthesis, for the first time, achieves chemically synthesis of uniform $Sm_2Fe_{17}N_3$ NPs.[17]

In summary, we present a general method to synthesize and stabilize REM based nanomagnets of $SmCo_5$, Sm_2Co_{17} and $Sm_2Fe_{17}N_3$ with ultra-large coercivities and high magnetic moments. The key feature of the synthesis is the controlled reductive decomposition of $Sm(acac)_3$ and $M(acac)_3$ (M = Co or Fe) into hexagonal CoO or cubic FeO with amorphous Sm_2O_3 embedded in the MO structure. Once these SmM-O are coated with CaO and organics on the NP surfaces are removed, the SmM-O can be reduced at 850 °C by Ca to $SmCo_5$, Sm_2Co_{17} and Sm_2Fe_{17} NPs. Further nitridation of Sm_2Fe_{17} at 600 °C leads to the formation of $Sm_2Fe_{17}N_3$ NPs. In the synthetic process, sizes and compositions of the oxide and REM based NPs are controlled by molar ratios of $Sm(acac)_3/M(acac)_3$. More importantly, these REM based NPs can be dispersed in ethanol, allowing their mixing with PEG and their magnetic alignment in the PEG matrix. The aligned 200 nm $SmCo_5$, 100 nm Sm_2Co_{17} and 100 nm $Sm_2Fe_{17}N_3$ NPs shows the room temperature H_c (M_s) of 49.2 kOe (88.7 emu/g), 24.2 kOe (100.5 emu/g), and 15.4 kOe (127.9 emu/g) respectively, all among the largest values ever reported for NPs of these materials. Our synthesis provides a viable avenue not only to high performance REM based nanomagnets, but also to NP-polymer composites that will be important towards fabrication of high performance permanent magnets, flexible magnets, and printable magnetic inks for magnetic and electronic applications.

Experimental Section

Experimental details are given in the Supporting Information.

Acknowledgements

This work was supported by the Critical Materials Institute, an Energy Innovation Hub funded by the U.S. Department of Energy, Office of Energy Efficiency and Renewable Energy, Advanced Manufacturing Office. Work at Lawrence Livermore National Laboratory (LLNL) performed under Contract DE-AC52-07NA27344. Part of electron microscopy work was carried out at the School of Chemical Engineering and Technology, Harbin Institute of Technology, which is supported by the National Natural Science Foundation of China under Grant No. 51571072, and the Center for Functional Nanomaterials, Brookhaven National Laboratory (BNL), which is supported by the DOE, Office of Basic Energy Sciences, under contract DE-SC-0012704.

Keywords: intermetallic phases • magnetic properties • nanoparticles • rare earths • reduction

[1] a) L. H. Wu, A. Mendoza-Garcia, Q. Li, S. H. Sun, *Chem. Rev.* **2016**, *116*, 10473-10512; b) O. Gutfleisch, M. A. Willard, E. Bruck, C. H. Chen, S. G. Sankar, J. P. Liu, *Adv. Mater.* **2011**, *23*, 821-842; c) Z. Y. Fei, B. Huang, P. Malinowski, W. B. Wang, T. C. Song, J. Sanchez, W. Yao, D. Xiao, X. Y. Zhu, A. F. May, W. D. Wu, D. H. Cobden, J. H. Chu, X. D. Xu, *Nat. Mater.* **2018**, *17*, 778-782.

[2] a) H. Zeng, J. Li, J. P. Liu, Z. L. Wang, S. H. Sun, *Nature* **2002**, *420*, 395-398; b) S. H. Sun, C. B. Murray, D. Weller, L. Folks, A. Moser, *Science* **2000**, *287*, 1989-1992; c) F. Liu, J. H. Zhu, W. L. Yang, Y. H. Dong, Y. L. Hou, C. Z. Zhang, H. Yin, S. H. Sun, *Angew. Chem. Int. Ed.* **2014**, *53*, 2176-2180; d) M. Suda, Y. Einaga, *Angew. Chem. Int. Ed.* **2009**, *48*, 1754-1757.

[3] a) W. B. Cui, Y. K. Takahashi, K. Hono, *Adv. Mater.* **2012**, *24*, 6530-6535; b) S. Sawatzki, R. Heller, C. Mickel, M. Seifert, L. Schultz, V. Neu, *J. Appl. Phys.* **2011**, *109*; c) R. Skomski, J. M. D. Coey, *Phys. Rev. B* **1993**, *48*, 15812-15816; d) O. Akdogan, H. Sepehri-Amin, N. M. Dempsey, T. Ohkubo, K. Hono, O. Gutfleisch, T. Schrefl, D. Givord, *Adv. Electron. Mater.* **2015**, *1*. 1500009

[4] S. C. Hong, J. I. Lee, Y. R. Jang, B. I. Min, A. J. Freeman, *J. Magn. Magn. Mater.* **1992**, *104*, 659-660.

[5] a) Z. H. Ma, S. X. Yang, T. L. Zhang, C. B. Jiang, *Chem. Eng. J.* **2016**, *304*, 993-999; b) D. Y. Li, H. Wang, Z. H. Ma, X. Liu, Y. Dong, Z. Q. Liu, T. L. Zhang, C. B. Jiang, *Nanoscale* **2018**, *10*, 4061-4067; c) Y. Zhong, V. Chaudhary, X. Tan, H. Parmar, R. V. Ramanujan, *Nanoscale* **2017**, *9*, 18651-18660; d) A. M. Gabay, X. C. Hu, G. C. Hadjipanayis, *J. Magn. Magn. Mater.* **2014**, *368*, 75-81; e) J. R. Li, Z. Xi, Y. T. Pan, J. S. Spendelow, P. N. Duchesne, D. Su, Q. Li, C. Yu, Z. Y. Yin, B. Shen, Y. S. Kim, P. Zhang, S. H. Sun, *J. Am. Chem. Soc.* **2018**, *140*, 2926-2932; f) L. Fang, T. L. Zhang, H. Wang, C. B. Jiang, J. H. Liu, *J. Magn. Magn. Mater.* **2018**, *446*, 200-205.

[6] a) Y. Hou, Z. Xu, S. Peng, C. Rong, J. P. Liu, S. Sun, *Adv. Mater.* **2007**, *19*, 3349-3352; b) H. W. Zhang, S. Peng, C. B. Rong, J. P. Liu, Y. Zhang, M. J. Kramer, S. H. Sun, *J. Mater. Chem.* **2011**, *21*, 16873-16876; c) Z. H. Ma, M. Yue, Q. Wu, C. L. Li, Y. S. Yu, *Nanoscale* **2018**, *10*, 10377-10382; d) B. Shen, C. Yu, D. Su, Z. Y. Yin, J. R. Li, Z. Xi, S. H. Sun, *Nanoscale* **2018**, *10*, 8735-8740; e) C. L. Li, Q. Wu, Z. H. Ma, H. H. Xu, L. Y. Cong, M. Yue, *J. Mater. Chem. C* **2018**, *6*, 8522-8527; f) B. Shen, A. Mendoza-Garcia, S. E. Baker, S. K. McCall, C. Yu, L. H. Wu, S. H. Sun, *Nano Lett.* **2017**, *17*, 5695-5698.

[7] W. S. Seo, J. H. Shim, S. J. Oh, E. K. Lee, N. H. Hur, J. T. Park, *J. Am. Chem. Soc.* **2005**, *127*, 6188-6189.

[8] K. M. Nam, J. H. Shim, D. W. Han, H. S. Kwon, Y. M. Kang, Y. Li, H. Song, W. S. Seo, J. T. Park, *Chem. Mater.* **2010**, *22*, 4446-4454.

[9] Q. Q. Qi, Y. Z. Chen, L. S. Wang, D. Q. Zeng, D. L. Peng, *Nanotechnology* **2016**, *27*.

[10] V. G. Harris, Y. Chen, A. Yang, S. Yoon, Z. Chen, A. L. Geiler, J. Gao, C. N. Chinnasamy, L. H. Lewis, C. Vittoria, E. E. Carpenter, K. J. Carroll, R. Goswami, M. A. Willard, L. Kurihara, M. Gjoka, O. Kalogirou, *J. Phys. D. Appl. Phys.* **2010**, *43*.

[11] D. G. Li, C. Wang, D. Tripkovic, S. H. Sun, N. M. Markovic, V. R. Stamenkovic, *Acs. Catal.* **2012**, *2*, 1358-1362.

[12] G. S. Chaubey, N. Poudyal, Y. Liu, C. Rong, J. P. Liu, *J. Alloy. Compd.* **2011**, *509*, 2132-2136.

[13] J. M. D. Coey, *Magnetism and magnetic materials,* Cambridge University Press, **2014** p. 400

[14] H. Kohlmann, T. C. Hansen, V. Nassif, *Inorg. Chem.* **2018**, *57*, 1702-1704.

[15] a) Y. Wang, Y. Li, C. Rong, J. P. Liu, *Nanotechnology* **2007**, *18*, 465701; b) N. Poudyal, C. B. Rong, J. P. Liu, *J. Appl. Phys.* **2010**, *107*; c) W. F. Li, A. M. Gabay, X. C. Hu, C. Ni, G. C. Hadjipanayis, *J. Phys. Chem. C* **2013**, *117*, 10291-10295.

[16] a) K. Takagi, H. Nakayama, K. Ozaki, K. Kobayashi, *J. Magn. Magn. Mater.* **2012**, *324*, 1337-1341; b) Q. L. Fang, X. X. An, F. Wang, Y. Li, J. Du, W. X. Xia, A. R. Yan, J. P. Liu, J. Zhang, *J. Magn. Magn. Mater.* **2016**, *410*, 116-122.

[17] a) Y. Hirayama, A. K. Panda, T. Ohkubo, K. Hono, *Scr. Mater.* **2016**, *120*, 27-30; b) S. Okada, K. Suzuki, E. Node, K. Takagi, K. Ozaki, Y. Enokido, *J. Alloy. Compd.* **2017**, *695*, 1617-1623.

Entry for the Table of Contents

Layout 1:

COMMUNICATION

A new chemical process is developed to prepare strongly ferromagnetic $SmCo_5$ nanoparticles (NPs) via controlled reduction of SmCo-O multipods. The 200 nm $SmCo_5$ NPs embedded in polyethylene glycol are aligned magnetically and show the room temperature coercivity of 49.2 kOe. The synthetic method has also been extended to prepare ferromagnetic Sm_2Co_{17} and $Sm_2Fe_{17}N_3$ NPs.

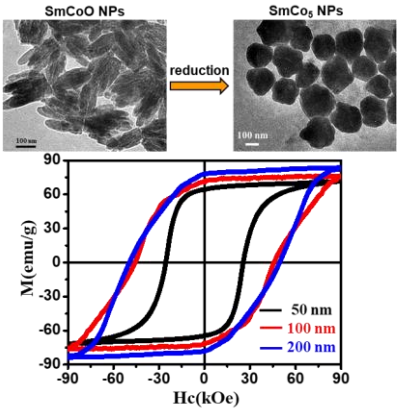

*Bo Shen, Chao Yu, Alexander A. Baker, Scott K. McCall, Yongsheng Yu, Dong Su, Zhouyang Yin, Hu Liu, Junrui Li and Shouheng Sun**

Page No. – Page No.

Chemical synthesis of magnetically hard and strong rare-earth metal based nanomagnets